NPL REPORT
DQL-RN 007

Pulse Shape Discrimination in Hydrogen Proportional Counters by Digital Methods

N P Hawkes

NOT RESTRICTED

SEPTEMBER 2004

Pulse Shape Discrimination in Hydrogen Proportional Counters by Digital Methods

N P Hawkes
Quality of Life Division

ABSTRACT

A fast digital sampler (waveform digitiser) has been used to measure the rise times and amplitudes of pulses from hydrogen - filled spherical proportional counters (type SP2). The rise time information allowed neutron events to be distinguished from gamma events, so that neutron data could be measured at energies below those possible with amplitude measurements alone. The associated electronics were considerably simpler than a conventional 2-parameter system.

Some of the rise time distributions show interesting features that would be missed by systems that analyse only the pulse height.

ISSN 1744-0629

National Physical Laboratory
Hampton Road, Teddington, Middlesex, TW11 0LW

Approved on behalf of Managing Director, NPL, by Dr Desmond MacMahon, Knowledge Leader, Radioactivity and Neutron Metrology Team, authorised by the Director, Quality of Life Division

Contents

Figures

Tables

1 Introduction

Neutron spectrometry is important in radiation protection, because the dose equivalent per unit fluence in a neutron field depends on the neutron energy, which means that the dose equivalent can depend strongly on the shape of the neutron spectrum. Bonner sphere spectrometers cover the entire energy range of interest, but the resolution is poor. Higher resolution measurements are desirable, particularly in the upper energy region of 10 keV – 20 MeV, where much of the dose equivalent usually occurs. Organic liquid scintillators are well suited for energies above about 1 MeV, but below this energy the signal becomes small relative to the noise, and neutron events become hard to distinguish from gammas. Accordingly, for energies from a few tens of keV up to about 1.5 MeV, gas-filled proportional counters are the preferred detector(1).

Detectors of this kind consist of a metal shell, usually cylindrical or spherical, filled to a pressure of about $10^5 - 10^6$ Pa (1 – 10 atmospheres) with a target gas such as hydrogen, helium or methane. A thin anode wire, maintained at high positive voltage, is stretched along the axis of the chamber. An incoming neutron may undergo an elastic scatter or a nuclear reaction with one of the gas nuclei (depending on the nature of the gas), and the recoiling charged particle or particles produce primary ionisation in the gas. When the primary electrons arrive within a few wire radii of the central wire, where the electric field is very large, gas multiplication takes place, and a large number of secondary ions are produced. It is the motion of these secondary ions that generates the electrical signal from the detector(2). The multiplication avalanche does not spread along the anode wire, as it does in a GM tube, and so the output signal remains proportional to the original primary ionisation.

One popular type of chamber is that known as 'SP2', originally developed by Benjamin *et al.*(3,4) This type of chamber is spherical (so that its response is almost independent of the direction of the incoming neutrons), and the gas filling is hydrogen. Hydrogen has the advantage that the (n, p) elastic scattering cross section is well known, and the spatial distribution of the recoiling protons is isotropic in the centre-of-mass frame at the energies of interest, which simplifies the calculation of the detector response. The chambers are 40 mm in diameter, and the walls are 0.5 mm thick stainless steel (see Figure 1).

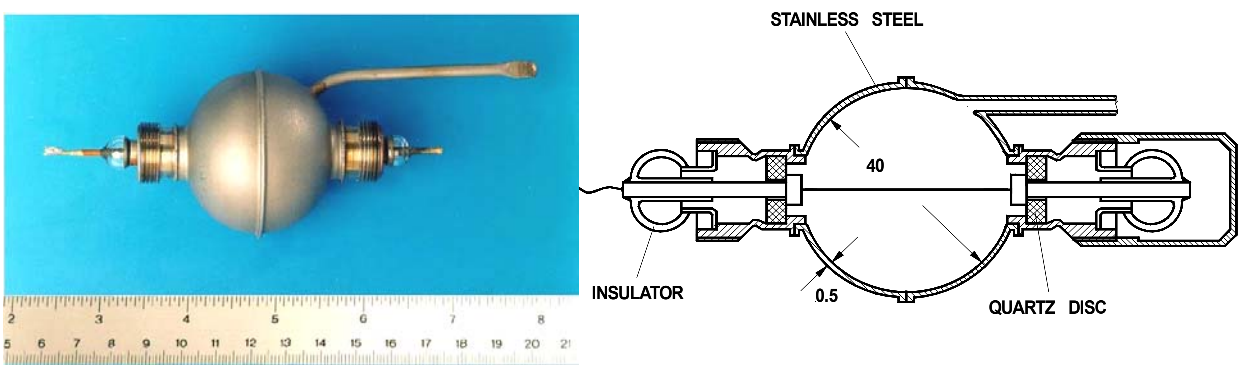

Figure 1. Construction of SP2 proportional counter. (Reproduced from Ref. (1))

NPL has several SP2 chambers, with pressures from $5 \times 10^4 - 10^6$ Pa (0.5 - 10 atmospheres). An original set was obtained from the University of Birmingham and was characterised by Tagziria and Thomas(5), and later some additional counters which had been characterised by Birch *et al.*(6) were added. Together, the chambers cover the energy range 50 keV – 1.5 MeV approximately. The upper limit is determined by the energy at which, even in the highest-pressure chamber, a substantial proportion of the proton tracks is cut short by the chamber wall. The lower energy limit occurs when, even in the lowest-pressure chamber, the pulse height spectrum becomes affected by the low amplitude signals from gamma rays.

The aim of this work was to reduce the lower limit below 50 keV by introducing neutron / gamma discrimination, so that gamma events could be identified and removed at the analysis stage.

2 Neutron / Gamma Discrimination in SP2 Counters

2.1 Discrimination by Amplitude

In SP2 counters, neutrons interact by scattering from a proton in the hydrogen gas filling (see Figure 2). The proton may acquire any energy up to the original neutron energy, and it produces primary ionisation along its track until it is brought to rest by the gas (or hits the wall of the chamber).

Gamma rays also interact in the chamber, and they do so mainly via the electrons in the chamber wall. An electron, given energy by the gamma ray (typically by a Compton interaction) enters the gas filling and generates ionisation as before, but the stopping power of the gas is such that the electron typically crosses the entire chamber and loses only part of its energy in the gas. Consequently there is a maximum energy that it can deposit in the gas, regardless of the original energy of the gamma ray. This energy, roughly 50 keV depending on the gas pressure, is the energy at which the electron range is just equal to the chamber diameter. Electrons with either less or more energy than this will deposit less energy in the gas.

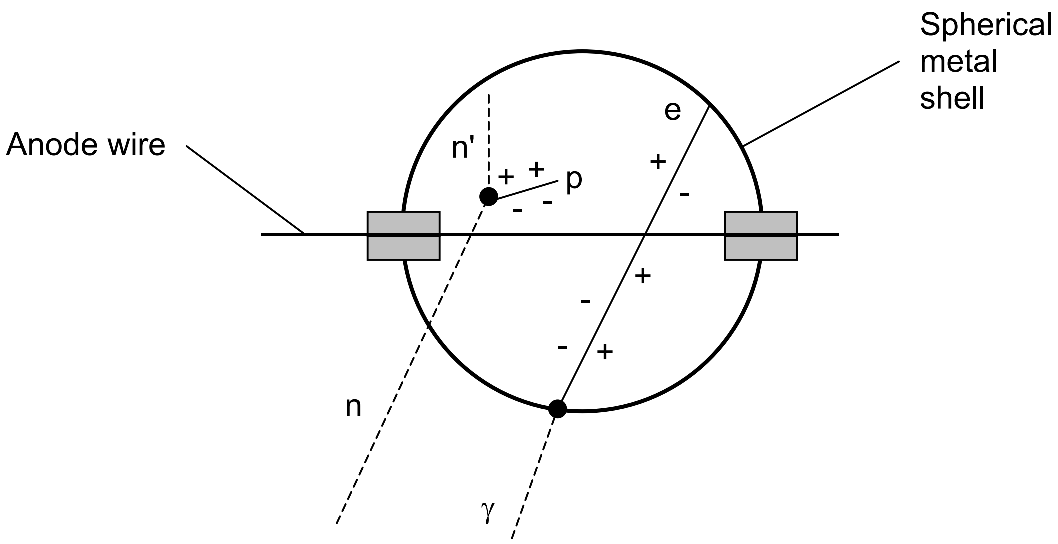

Figure 2. Schematic showing neutron and gamma interactions in SP2 chamber.

An easy and effective means of gamma discrimination is therefore possible by simply setting a threshold just above the maximum gamma pulse energy. Of course, neutrons below this threshold cannot then be observed at all.

2.2 Discrimination by Pulse Rise Time

The aim of the present work was to investigate how to make use of neutron signals below the maximum gamma pulse energy, and for this a different approach is necessary. Fortunately it is possible to make use of the difference in rise time between neutron and gamma pulses.

Kinetic Energy, MeV	Ranges in Hydrogen, mm (Continuous slowing down approximation)					
	1 atmosphere		3 atmospheres		10 atmospheres	
	Protons	Electrons	Protons	Electrons	Protons	Electrons
0.050	2.2	235	0.7	78	0.2	24
0.100	3.8	794	1.3	265	0.4	79
0.200	8.0	2530	2.7	843	0.8	253
0.500	31.0	10100	10.3	3380	3.1	1010
1.000	101.0	25300	33.7	8430	10.1	2530
1.500	206.0	41000	68.8	13700	20.6	4100
2.000	344.0	56600	115.0	18900	34.4	5660

Table 1. Ranges of protons and electrons in hydrogen.
(Calculated from the data of Berger et al[7] and given to 3 significant figures max.)

Table 1 shows the ranges of protons and electrons of various energies in hydrogen gas. The values are much lower for protons than for electrons of the same energy, that is to say the ionisation tracks will be much shorter for protons than electrons (indeed, electrons typically cross the entire chamber). The primary ionisation electrons created along the length of an ionisation track typically produce no significant contribution to the output signal until they reach the narrow multiplication zone around the central anode wire, and generate secondary ionisation. So if the original particle track is short, the primary electrons will all arrive at the anode within a short span of time, and the pulse rise time will be short. If on the other hand the particle track is long, there is likely to be a large spread of arrival times and hence a long rise time in the total output pulse. Therefore, neutrons will produce pulses with short rise times (about a microsecond or less), while gamma rays will produce pulses with rise times of up to about four microseconds[1].

It is interesting to note the differences between neutron / gamma pulse shape discrimination (PSD) in proportional counters and that in organic liquid scintillators such as NE213. In the former case, discrimination is based on the difference in path length between protons and electrons, and the discrimination information is in the rise time of the pulse. In the latter case, discrimination is based on the different proportions in which protons and electrons excite scintillator components of different lifetimes, and the discrimination information is in the fall time of the pulse.

Several different techniques for rise time PSD have been used in SP2 data acquisition systems. (See, for example, Refs. 8 - 11.) Most involve fanning out the signal from the chamber into two processing chains, one to determine the total ionisation using conventional spectroscopy electronics, and the other to measure the rise time with (for example) a shaping amplifier tuned to appropriate time constants, or a pair of discriminators and a time-to-amplitude converter. The two signals are then acquired in coincidence in a dual-parameter multi-channel analyser (MCA).

Recently, however, fast digital samplers (waveform digitisers) have become available which are easily capable of sampling the preamplifier output from an SP2 chamber frequently enough to record the shape of the rising edge adequately. The main advantages of this approach are:

- The electronics are greatly simplified. The digitiser processes the preamplifier pulse directly (except possibly for some shape-preserving amplification to match the pulse height to the input range of the digitiser). Furthermore, the analysis algorithm can derive both the pulse amplitude and the rise time from the same acquired pulse shape, so there is no need for two processing chains or a dual-parameter MCA.
- The rise time is measured directly from the preamplifier pulse, and not via a shaping amplifier tuned to respond to rise times.
- The analysis algorithm can in principle be tailored for greatest effectiveness in the particular experimental set-up in use. For example, pile-up detection and / or recovery may be introduced.
- Depending on counting rates, it may be possible to store the captured waveforms for later analysis. This allows the use of complex analysis algorithms, too slow for use in real time, or the raw data can be repeatedly re-processed to compare the effects of different analysis techniques.

There are of course also some disadvantages to the new approach:

- If the experimenter decides to store the waveforms, a great deal of data may be generated in a short time. An 8-bit sampler running at 1 GHz (1 sample per ns) has a peak rate of 1 GByte/s, but even assuming a much lower average rate of 25 MB/s (approximately the maximum practical rate in a PC), a ten-minute measurement would still produce 15 GB.
- If, on the other hand, the data are analysed as they are acquired, and only the results are stored, the ability to re-analyse is lost.
- Conventional electronics are carefully designed to eliminate unwanted signals, through the use of shaping time constants for example. A basic digitiser lacks such filtering, and if unwanted signals are a problem the experimenter must add a hardware filter in front of the digitiser, or make careful use of the triggering options provided on the digitiser, or carry out filtering in software during the analysis.

In the present work, the decision was made to carry out the PSD by digital means, in order to simplify the electronics, make the rise time measurements directly, and gain experience in this novel and interesting technique.

3 Experimental Measurements

3.1 Measurements of built-in calibration source

3.1.1 Purpose of the measurements

There are several reasons why the expected neutron / gamma rise time differences may be difficult to see in practice. For example, if a gamma ray produces an electron that travels through the chamber parallel to the anode wire, the rise time will be short even though the track is long, because all parts of the track are the same distance from the wire. Also, many of the popular and convenient isotopic neutron sources (e.g. ^{241}Am/Be) have a significant proportion of their spectrum above 2 MeV[(12)], and at these energies the protons are able to cross the chamber (see Table 1) and therefore have the same path length as a typical electron.

So the decision was taken to start the investigation with a much simpler case. The NPL 1-atmosphere counter SP2-1[(5)] has a small ^{239}Pu alpha emitter at the centre of the axial wire, to provide a rough calibration and a check of normal operation. The energy of the alphas (5.2 MeV) is such that they do not stop in the gas but reach the chamber wall, having deposited enough energy in the gas to produce a pulse well above the noise. The geometry is therefore as shown in Figure 3, with all tracks starting at the centre of the chamber and running for the same distance. An approximation to the corresponding rise time distribution can be readily calculated if one assumes that the drift velocity of the primary ionisation electrons is constant, and that they always travel towards the closest part of the wire. (The first assumption in particular is not realistic, as the electric field strength in the chamber is far from uniform[(13)], but it does allow the calculation to be done straightforwardly).

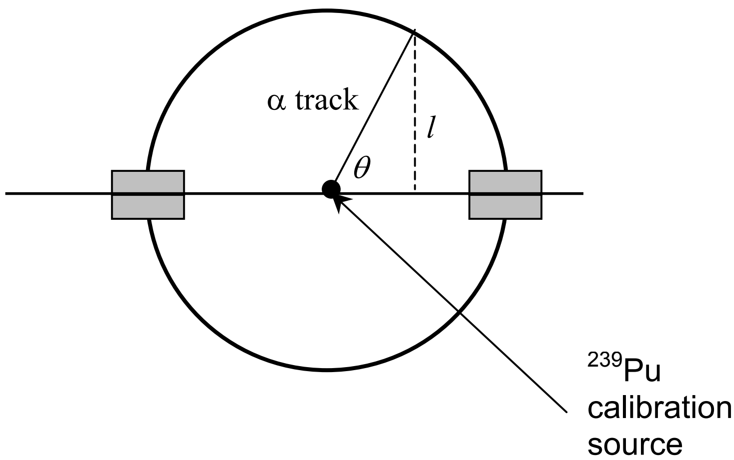

Figure 3. Geometry of tracks from calibration source.

Under these assumptions, the rise time for a particular track will be proportional to the distance l of the end of the track from the wire. This distance is proportional to $\sin(\theta)$, where θ is the angle between the wire and the alpha track.

As the direction of the alpha track is random, the probability of seeing an angle between θ and $\theta + d\theta$ is proportional to $\sin(\theta)d\theta$, and the distribution of rise times *t* evaluates as

$$N(t)dt = K\frac{t\,dt}{\sqrt{T^2 - t^2}} \qquad (1)$$

where *K* is a normalisation constant and *T* is the maximum rise time, i.e. the rise time for a track that leaves the source at right angles to the wire.

3.1.2 Experimental setup

The hardware used to measure the rise time distribution experimentally is shown in Figure 4. The digital sampler used for the measurements was the ANSTO / NPL Digital Coincidence Counting (DCC) system[(14)]. This system was developed to determine the activity of ionising radiation samples by beta – gamma coincidence counting, but with its 20 MHz sampling rate (50 ns between samples) and 12-bit resolution it is well suited to measuring rise times of the order of microseconds.

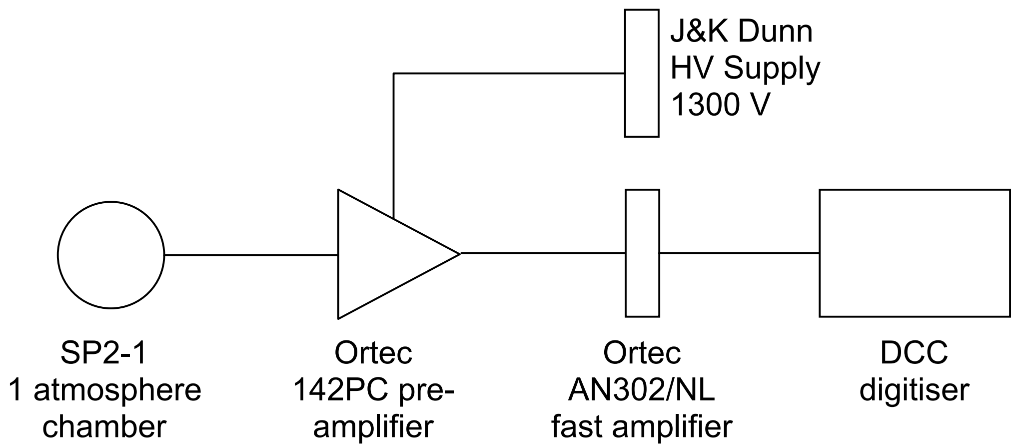

Figure 4. Electronics for rise time measurements on alpha source

The fast amplifier has a fixed gain of approximately 4.5. It does not perform any shaping, but was simply used to match the amplitude of the pre-amplifier output to the 0 – 1 V input range of the DCC system. The maximum output voltage from the amplifier, at which the response is still linear, is 1 V.

The DCC system starts sampling as soon as the input voltage exceeds the threshold (8 mV for the present measurement), and continues at 20 MSamples / s until the input voltage drops below the threshold again. The samples are written to a binary disc file along with header information identifying the start of each pulse. In the present experiment, a 2-hour run produced an 88 MB file containing about 13,000 alpha pulses.

Analysis software was written to read the raw DCC file, list the pulse samples out in a text file, and derive the rise time distribution. Figure 5 shows the initial portion of a typical captured alpha pulse; it peaks at about 3 – 4 microseconds (so that the rising edge is covered by about 60 – 80 samples), and then decays much more slowly with time constants characteristic of the preamplifier.

The preamplifier, combined with the fast amplifier, introduced a baseline offset of about – 0.1 V. As voltages below zero are not digitised by the DCC, the lowest part of the pulse shape was absent in each case, so for most pulses the conventional 10% to 90% rise time was not available. However, the 40% point was available for even the lowest alpha pulses (at about + 0.2 V), so the 40% to 90% rise time was evaluated instead, using the known value of the offset to find the true position of the pulse baseline.

3.1.3 Experimental results

The measured rise time distribution is shown in Figure 6. The shape shows an increasingly steep rise up to a maximum at about 2.2 μs, followed by a rapid drop. The Figure also shows the theoretical distribution derived above (Eqn. 1), with the T parameter set to 2.2 μs and the normalisation set to match the area of the measured distribution below 2.2 μs. The two shapes agree reasonably well, suggesting that the gross shape of the measured distribution can be understood in terms of the simple geometry of Figure 3. The observed cutoff and peak at low rise times cannot be explained in this way, and probably confirm that the model used to derive the theoretical distribution is over-simplified.

The analysis algorithm derived the pulse amplitude as well as the rise time, and it is interesting to draw a scatter plot of rise time versus amplitude (Figure 7). A 3-dimensional plot of the same data is also shown (Figure 8); here the relative number of counts in each region of the amplitude – rise time plane is shown explicitly. The boundaries of the populated region of the plane are strikingly sharp, and this sharpness must derive from properties of the chamber, as only the right hand (1000 mV) boundary was imposed by the measurement system. Most of the counts are in the region of 350 mV and 2.2 μs, but there is a secondary peak (corresponding to the low pulse height peak in Figure 6) at about 250 mV and 0.5 μs. This peak appears to have been skewed to low pulse heights, perhaps because the low rise time pulses will be those in which the track lies close to the anode wire, and which will therefore experience the most distorted electrical fields.

Points continue to appear, with decreasing frequency, right up to the high amplitude side of the amplitude axis (right hand side of the graphs). This can be understood as a consequence of alpha particles leaving the source with reduced energy, due to slowing down in the wire or in the ^{239}Pu layer itself. Such alphas will deposit slightly more energy in the gas than the full energy alphas, because of the increase in stopping power with decreasing energy (recall that the alphas easily reach the chamber wall).

Projecting the distribution of Figure 8 onto the rise time axis would give the total measured rise time distribution of Figure 6, while projecting onto the amplitude axis would give a conventional pulse height spectrum. From the interpretation of the high amplitude points suggested in the previous paragraph, one would expect slices of constant amplitude to show a rise time distribution similar to Figure 6, as alphas at each emission energy generate their own rise time distribution in the manner of Figure 3, and the data do tend to support this.

It is clear that a great deal of interesting information is contained within the rise time distribution. This information is lost when the signals are processed with conventional spectrometry electronics only.

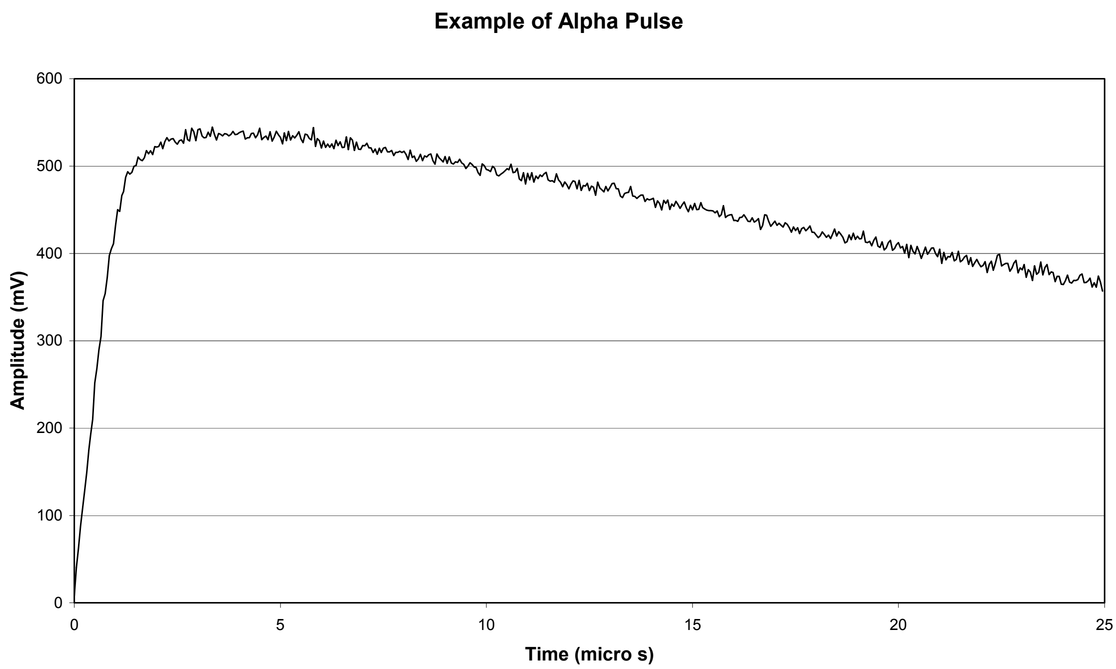

Figure 5. Typical pulse shape from the calibration source

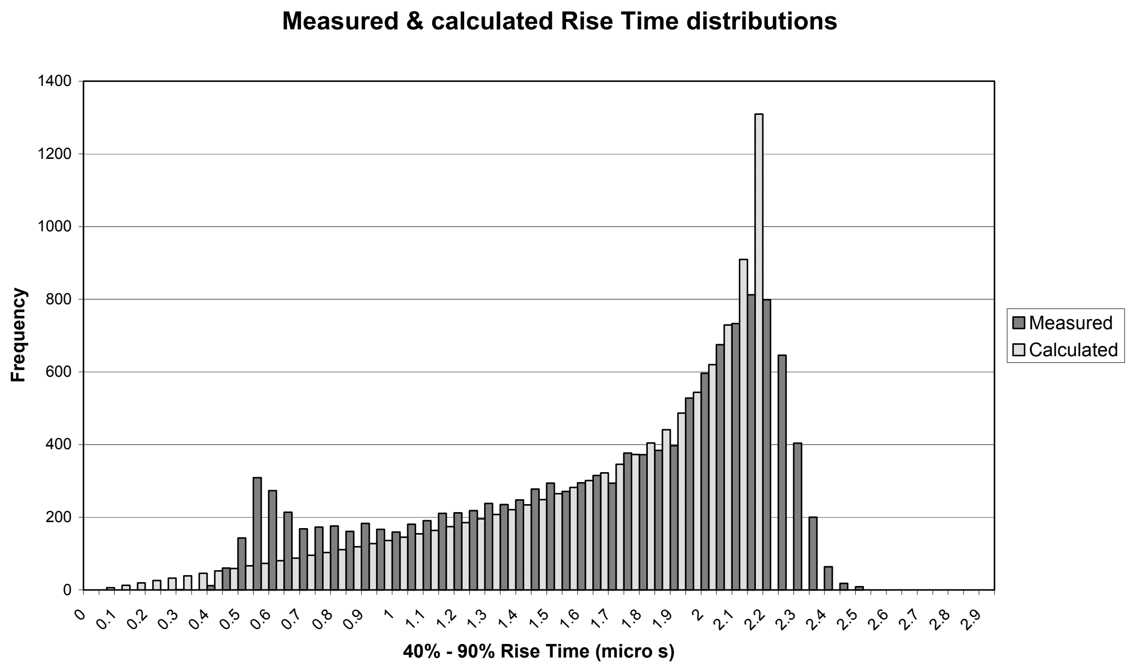

Figure 6. Rise time distribution from the calibration source (compensated for baseline offset), compared with the normalised theoretical distribution with T = 2.2 μs

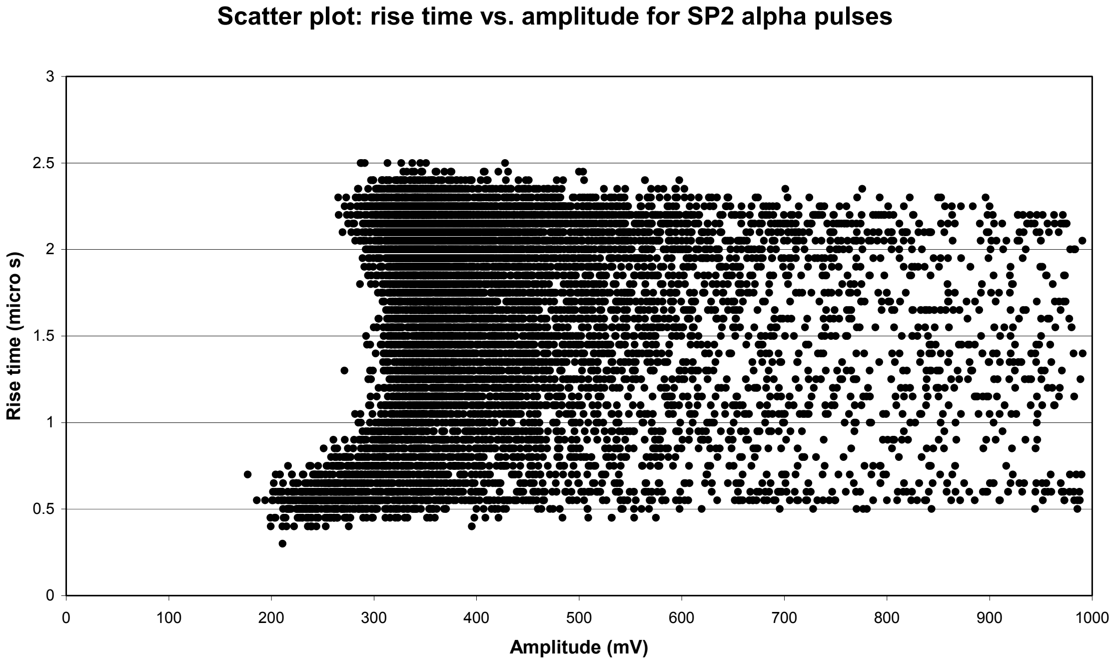

Figure 7. Scatter plot showing the rise time and amplitude of pulses from the alpha calibration source.

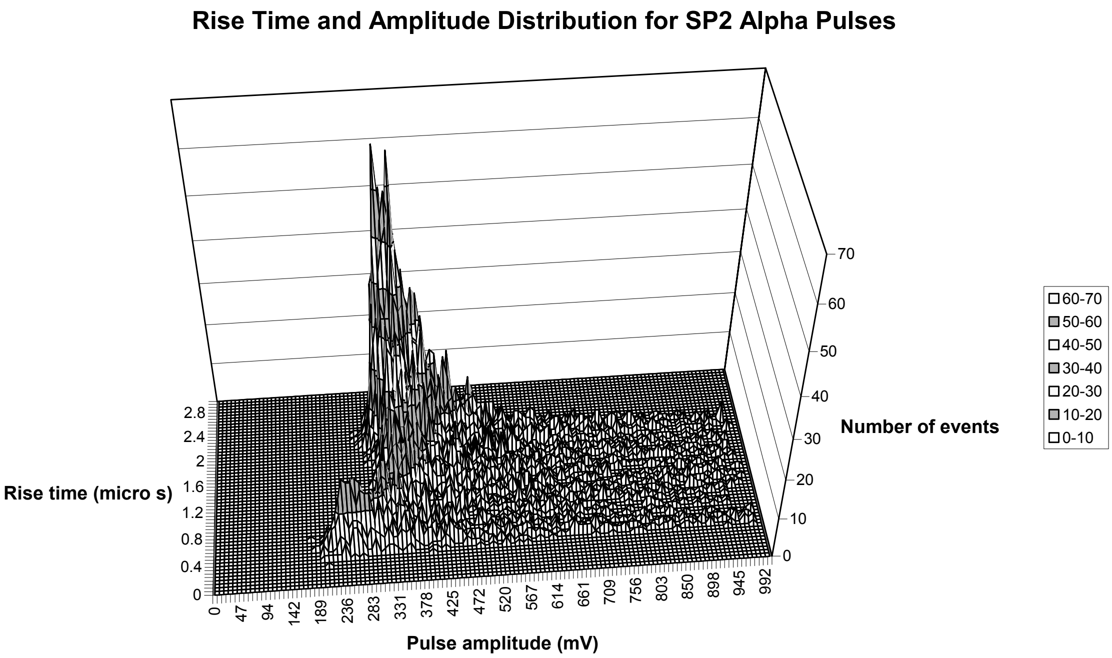

Figure 8. 3-dimensional version of previous Figure.

3.2 Measurements with neutrons and gammas

3.2.1 Experimental setup

Following the successful use of digital rise time analysis in the simple case of the internal calibration source, the technique was then applied to mixed neutron / gamma fields.

The negative baseline offset produced by the preamplifier and fast amplifier seemed likely to cause significant problems with the analysis of neutron and gamma signals, both of which are typically much smaller than the alpha signals. Also, the DCC system was found to be prone to errors, causing it to abandon data acquisition, when processing preamplifier pulses from a proportional counter exposed to a neutron source (a task it was not designed to perform). It is understood that the large number of low-amplitude pulses, coupled with the long decay time from the preamplifier, was filling the DCC system's memory buffer.

The decision was therefore taken to use a Tektronix TDS 5052 Digital Phosphor Oscilloscope in place of the DCC system. The oscilloscope has a greater maximum sampling frequency than the DCC system (5 GHz instead of 20 MHz), and (being a general purpose instrument) a much wider range of acquisition options. It can also digitise negative as well as positive input voltages. Its vertical resolution is 8 bits instead of 12, but this is adequate for the present measurements.

The oscilloscope has the built-in ability to make measurements on acquired pulse shapes, including amplitude and rise time as required here. (For the present work, the rise time algorithm was set up to measure the 10% to 90% transition time.) The instrument is also able to export pulse shapes and / or measurement results via a General Purpose Interface Bus (GPIB) connection, and software to allow such transfers to a Microsoft Excel spreadsheet is provided. The advantage of using the measurement facility and the transfer software supplied with the instrument are that the measurement results are available without programming effort, and that the waveforms need not be stored, so that the volume of data to be handled is quite modest. Of course, the ready-made software is not optimised for any particular application, and if waveforms are not stored (as they were not in the present experiment), they are not available for later additional study or re-analysis.

Initially, SP2 chambers with pressures of 9×10^5 – 10^6 Pa (9 - 10 atmospheres) were used, in order to maximise the difference between proton and electron path lengths and give the greatest neutron / gamma differences. Lower pressure chambers are more usual for the low-energy neutron measurements for which gamma discrimination is required, and 1 - 3×10^5 Pa (1 - 3 atmosphere) chambers were substituted in later measurements.

The electronics were very similar to those used previously, except that an Ortec 459 HV module was substituted for the J&K Dunn unit when the latter became unavailable. An Ortec 448 Research Pulser was added for some runs to test the resolution of the system.

The 5052 oscilloscope has a great many options for acquisition and measurement. Most of the measurements reported here were carried out using the parameters set out in Table 2.

The SP2 chamber was set up in the experimental area along with its preamplifier (connected via a short cable), with a signal lead about 80 m long connecting the preamplifier to the fast amplifier in the counting room. The signal from the preamplifier

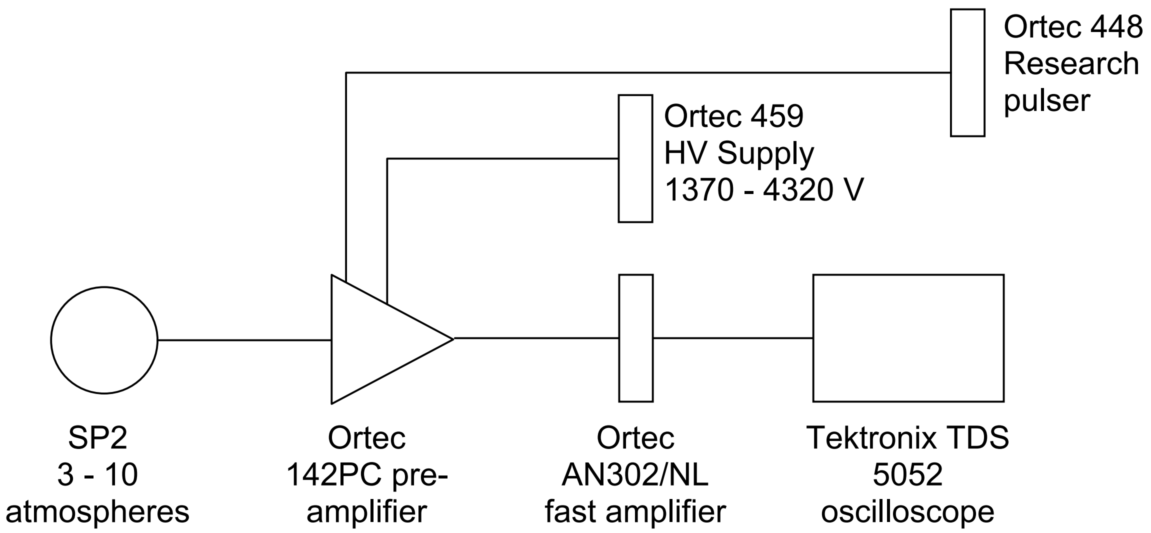

Figure 9. Electronics used with Tektronix 5052 oscilloscope

Parameter	Value
Horizontal scale	4 μs / division
Sampling frequency	125 MS/s (8 ns between samples)
Vertical scale	Usually 40 to 200 mV / division
Vertical position	0 to -3 divisions
Vertical offset	0 volts
Trigger	Usually Transition trigger, requiring the input to cross from 0 to 10.4 – 40 mV (depending on signal amplitude) in < 20 μs (see text).
Trigger position	20%
Trigger mode	NORM or AUTO
Acquisition mode	Sample (no averaging)
Channel	Channel 1
Coupling	AC
Termination	1 MΩ, but 50 Ω added externally.
Bandwidth	Limiter on: 20 MHz.

Table 2. Oscilloscope acquisition parameters

proved very susceptible to interference, even with low loss, well screened cable (Huber + Suhner type SX 07262 BD). Bursts of 2.4 MHz oscillations at 12 kHz caused particularly severe problems initially, but eventually this interference was traced to a stepper motor controller and eliminated. However, other unwanted signals remained, most notably a low frequency oscillation of about 100 mV in amplitude. At the timebase settings of interest, this caused the baseline to appear to jitter rapidly up and down on the oscilloscope screen by approximately ± 100 mV, an amount comparable to the amplitude of the pulses from the chamber. Setting the oscilloscope to AC coupling eliminated the jitter completely but also distorted the pulse shapes significantly. This was because the high pass cutoff frequency for AC coupling on this oscilloscope is 200 kHz when the input impedance is set to 50 Ω, and this frequency corresponds to rise times of around 1 –2 microseconds, i.e. it encroaches significantly on the range of rise times under study. It was therefore necessary to set the input impedance to 1MΩ, for which the cutoff frequency for AC coupling is 10 Hz, and add an external 50 Ω terminator. The much lower cutoff frequency left the pulses undistorted, but was also much less effective at reducing the jitter.

The baseline jitter made it hard to set a simple threshold trigger for the oscilloscope. Instead a Transition trigger was set up, which triggered acquisition when the input crossed between two adjustable thresholds in less than 20 microseconds. The lower threshold was always set to 0 mV, and the upper threshold to 10.4 – 40 mV depending on the amplitude range to be studied. This proved quite effective at avoiding unwanted triggers.

The trigger position was set at 20% of the horizontal axis of the graticule, in order to capture some of the quiescent baseline along with each pulse. This allowed the measurement algorithms to identify the zero voltage level each time.

As the shortest rise times of interest (about 1/20 microsecond) correspond to a frequency of only about 7 MHz, the oscilloscope's bandwidth limiter was activated and set to its lowest limit of 20 MHz.

The data transfer software was set up to transfer the measured values of the amplitude, fall time and rise time of each sampled pulse to a copy of Microsoft Excel previously installed on the oscilloscope itself. The two options for data capture are 'triggered' (in which data are transferred after each trigger) and 'timed' (in which data are transferred at regular intervals of 1 or more seconds). The 'triggered' option seemed the better initially, especially for measurements in which the counting rate was low, but this mode is unfortunately restricted to 256 acquisitions (the maximum number of columns in an Excel spreadsheet). For most measurements, the 'timed' mode was used, and duplicate data (produced if no new trigger took place during the timed interval) removed later in analysis.

Data that could not possibly be genuine preamplifier pulses were removed during analysis. Acceptance criteria were typically:

- Amplitude at least 4 mV and at most 200 – 1000 mV (depending on the amplitude range being studied)
- Rise time between 0.01 microseconds and 1 s.
- Data not a duplicate of the previous pulse.
- Fall time at least twice the rise time, where a valid fall time was available. (Typically, no valid fall time value was recorded, because the voltage level did not fall sufficiently far during the acquisition interval.)

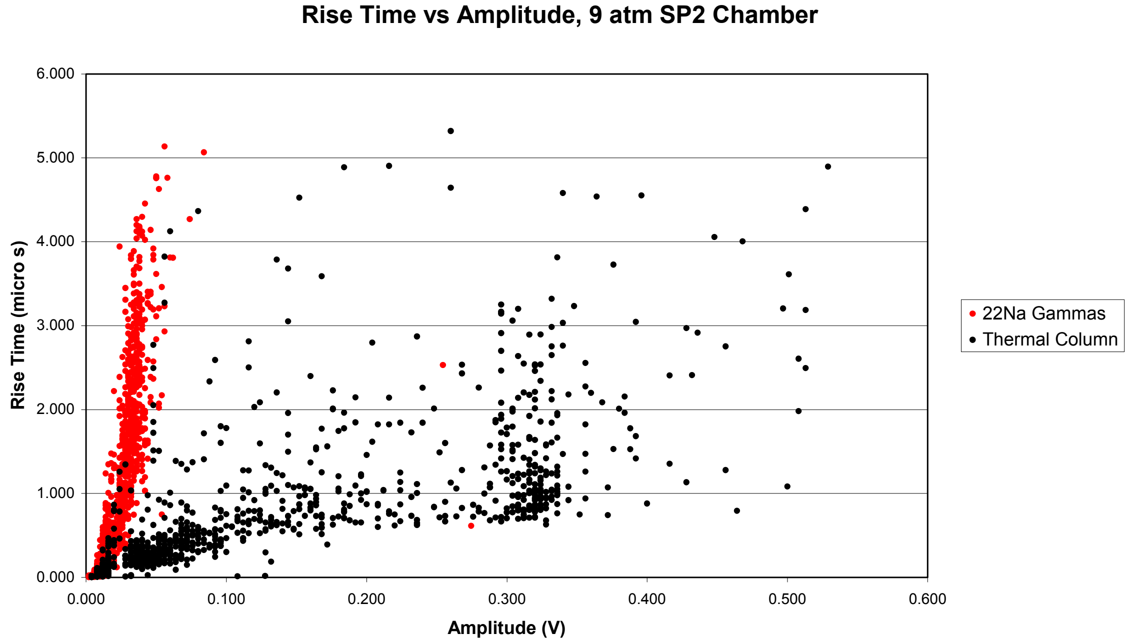

Figure 10. Results from the NPL 9-atmosphere chamber set up in the basement beneath the Thermal Column. Red dots: ^{22}Na gamma source beside the chamber. Black dots: Thermal Column operating.

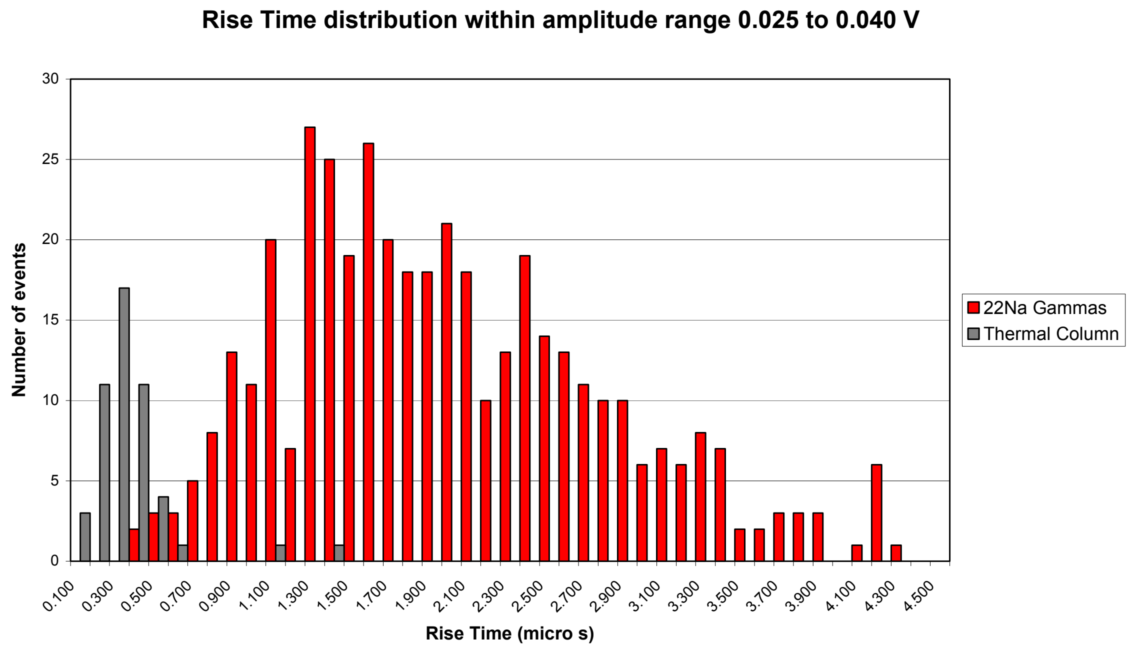

Figure 11. Rise time distribution from previous Figure, for the amplitude range 25 – 40 mV (60 – 96 keV approx) only.

3.2.2 Results with 9-atmosphere chamber

Figure 10 shows results from the NPL 9-atmosphere SP2 chamber[(5)], set up in a basement room beneath the NPL Thermal Neutron Facility[(15, 16)]. The black dots show data obtained while the facility was running, and the red dots show data obtained with a 37 kBq (10 microcurie) ^{22}Na source beside the chamber. The red dots exhibit the distribution expected for gamma events, namely low amplitude with a definite upper limit, and a high maximum rise time. The black dots have an amplitude peak at about 300 mV, and cannot therefore be (n, p) scattering events, for which the amplitude distribution must always decrease as amplitude increases. Instead they are assumed to be thermal events from the trace of ^{3}He gas that is commonly added to SP2 counters (including the particular one used here) for calibration. The ^{3}He(n, p)T reaction has a large thermal cross section, and deposits its Q value of 764 keV in the gas, giving an easily recognisable peak. Only three quarters of the energy is carried by the proton, the rest being carried by the triton, so the total ionisation track is slightly shorter than that which would be produced by a 764 keV proton alone. Nevertheless, the two distinct loci in Figure 10 represent successful n / gamma discrimination on the basis of rise time. This is shown more clearly in Figure 11, which plots the rise time distribution for Figure 10 data which lie in the narrow amplitude range 25 – 40 mV only (approximately 60 – 96 keV, based on the position of the 764 keV ^{3}He peak).

3.2.3 Results with 10-atmosphere chamber

The 10-atmosphere chamber from the set described by Birch *et al.*[(6)] was set up in the experimental area of the NPL Van de Graaff accelerator. In initial measurements with a ^{252}Cf source (identifier 4774 NE), no gamma ray locus was observed in the Amplitude / Rise Time plane when the chamber was operated at the recommended voltage of 3400 V. It seemed likely that this was because of the low gas gain of 2.4 at this voltage (compared with gas gains of 15 – 20 for the lower pressure chambers). Birch *et al.* recognised that this voltage might be less than optimum, but were concerned about the chamber insulation. In order to observe gamma events, the chamber voltage was increased in stages and the ^{252}Cf measurement repeated, until, at 4320 V, a gamma locus was clearly visible. This voltage was then adopted as the operating voltage for this chamber for the present work.

Figure 12 shows the data obtained when the chamber was placed 103.2 cm in front of a LiF target and exposed to 565 keV monoenergetic neutrons from the ^{7}Li(p,n) reaction at 0°. The edge of the proton recoil distribution is visible at about 320 mV, and events due to the gamma rays that inevitably accompany the neutrons can be seen at low amplitudes and high rise times.

A neutron / gamma discrimination boundary, in the form of a single sloping line together with an amplitude threshold, was set up as shown in the Figure, and then used to sort the events into separate neutron and gamma amplitude distributions. Points above the amplitude threshold were sorted by classifying those below the sloping line as neutrons and those above as gammas. (Points below the threshold cannot be sorted in this way because of the portion where the neutron and gamma loci overlap.) The results are shown in Figure 13. The proton recoil edge in the neutron amplitude distribution has a resolution of about 39% (based on the amplitude difference between the 87.5% and 12.5% points), which is much greater than Birch *et al.*'s result of 15% for this counter at 551 keV, measured using conventional spectroscopy electronics. (It should be borne in mind when considering these figures that the Birch *et al.* value is derived from a fitting procedure, and may not be directly comparable with the 87.5% - 12.5% value.)

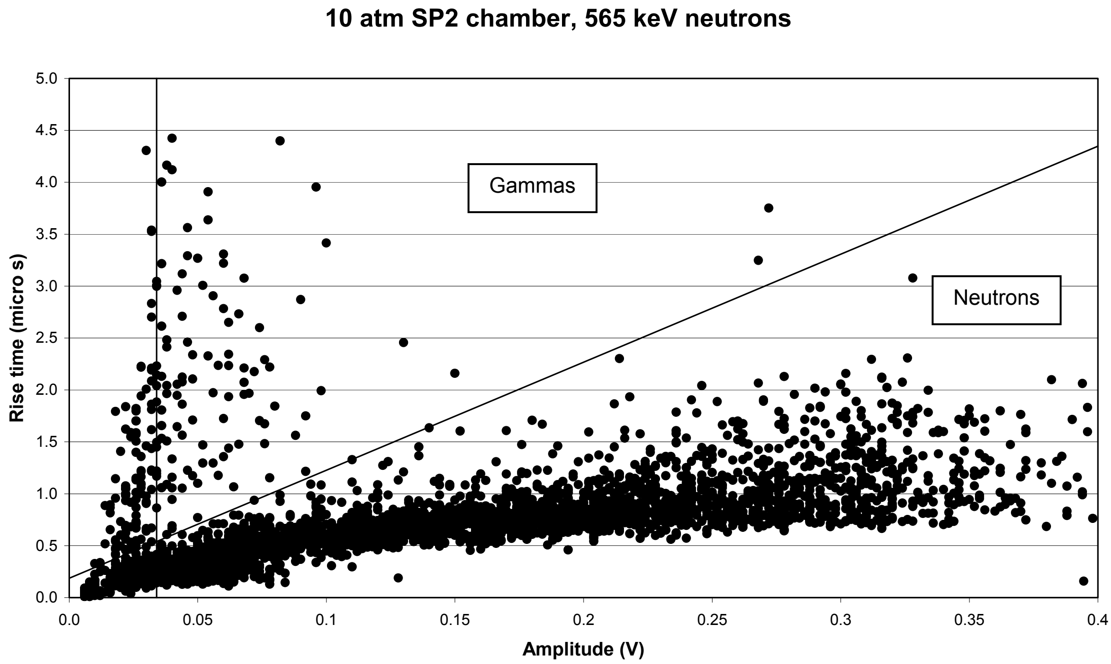

Figure 12. Data from 10 atmosphere SP2 chamber exposed to 565 keV neutrons. The lines show the neutron / gamma boundary used in subsequent analysis.

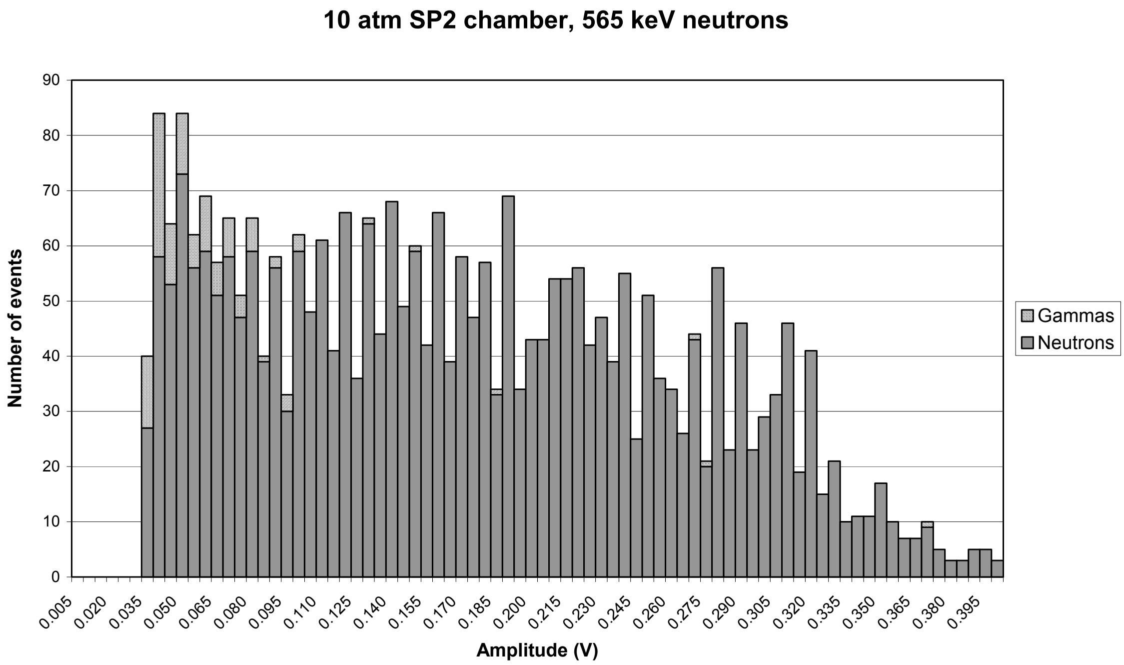

Figure 13. Amplitude distribution, with separated neutron and gamma contributions, for the 10 atmosphere SP2 chamber exposed to 565 keV neutrons.

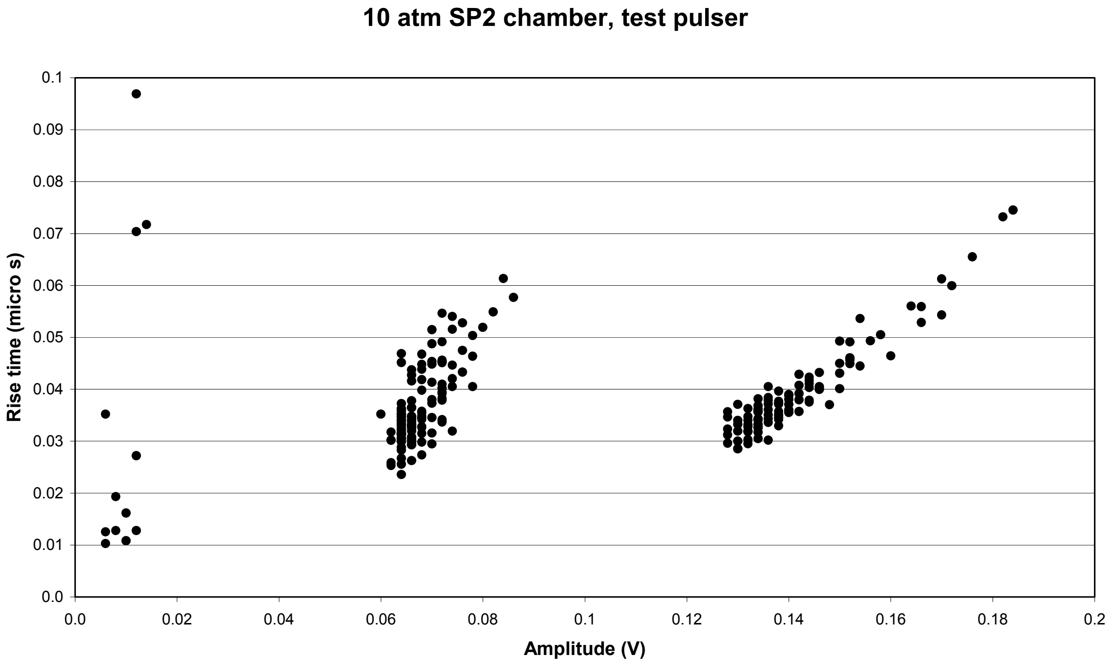

Figure 14. Test pulses measured with 10 atmosphere chamber connected. The rise time was set to 20 ns, with the two amplitudes differing by a factor of two.

To investigate the electronic resolution of the system, an Ortec 448 test pulser was connected to the preamplifier 'Test' input, and pulses injected at two amplitudes differing by a factor of two. The pulse rise time was set to 20 ns. The spread in the measured data (Figure 14) is about ± 10 mV for the lower peak. Normally one would expect the pulser resolution to be independent of pulser amplitude, but Figure 14 suggests some amplitude dependence. If the spread is proportional to amplitude, then the resolution of the proton recoil edge is roughly comparable with the pulser data, suggesting that the spread is dominated by the electronics and the measuring method and not by the chamber itself (despite the overvoltage). The amplitude difference between the two pulser peaks is about a factor of two, as expected, but the measured rise times are quite spread out and somewhat larger than the value set on the pulser unit. The high measured value may show the effect of the round trip from the pulser to the preamplifier and back to the oscilloscope, but the spread is of rather more concern.

3.2.4 Results with 3-atmosphere chamber

The 3-atmosphere chamber from the set described by Birch *et al.*(6) was placed at 247.6 cm from the LiF target and exposed to 144 keV monoenergetic neutrons from the ^{7}Li(p,n) reaction at 0°. This time, even when the chamber was operated at its recommended voltage of 2200 V, there was no problem in seeing the locus of low amplitude, high rise time events expected from the accompanying gammas.

At this stage it was thought prudent to reconfirm that this locus was indeed due to gamma events. Data were taken with just a 37 kBq (10 microcurie) ^{22}Na gamma source beside the chamber, and these are shown in Figure 15 superimposed on the data taken with 144 keV neutrons from the Van de Graaff. The ^{22}Na points clearly occupy the same region of the Amplitude / Rise Time plane as the high rise time locus in the Van de Graaff data. Also shown in Figure 15 are background data taken with no source near the chamber. These include a locus distinct from both the gamma and neutron data, at

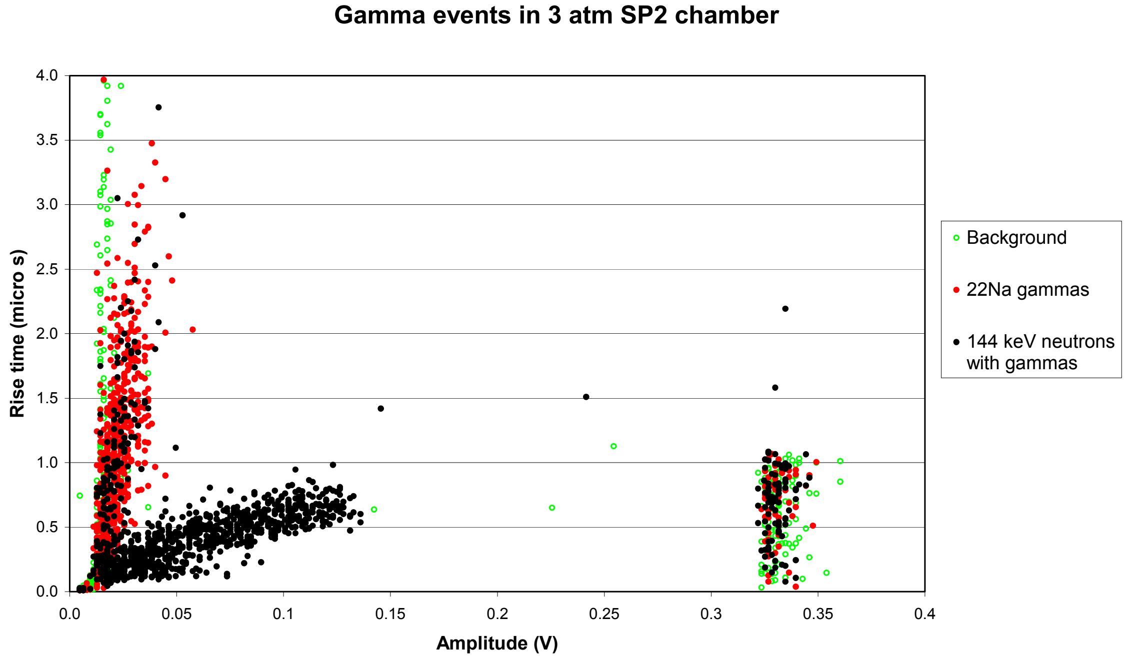

Figure 15. Confirmation that the high rise time, low amplitude events can be identified with gammas.

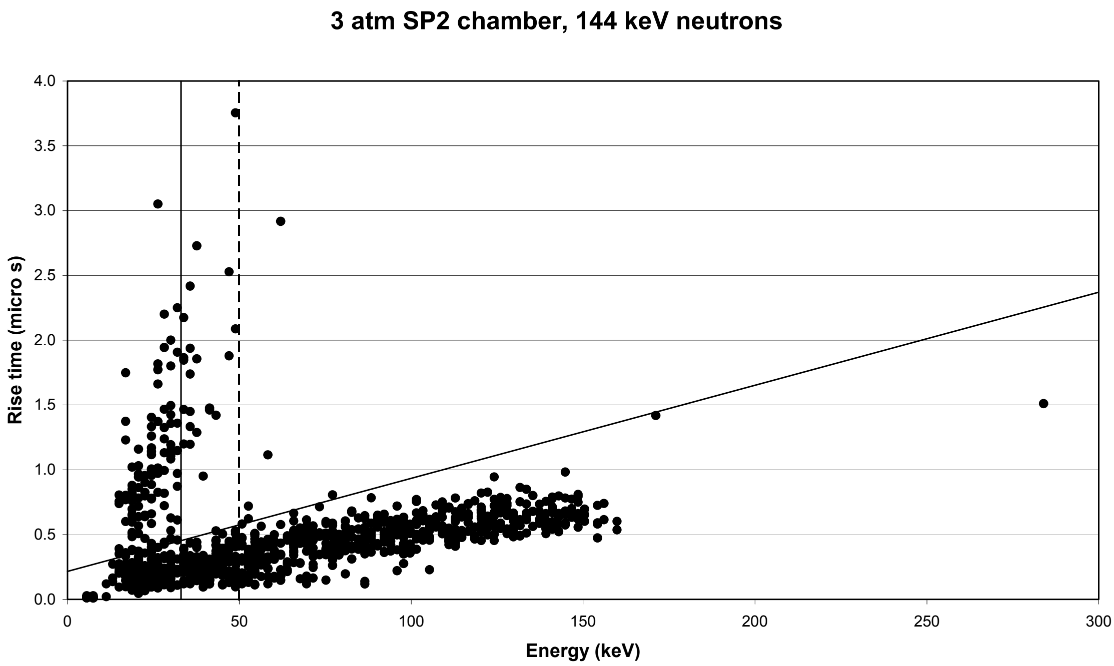

Figure 16. Data from 3 atmosphere SP2 chamber exposed to 144 keV neutrons. The solid lines show the neutron / gamma boundary used in subsequent analysis. The dashed line shows the approximate position of a discrimination boundary based only on amplitude.

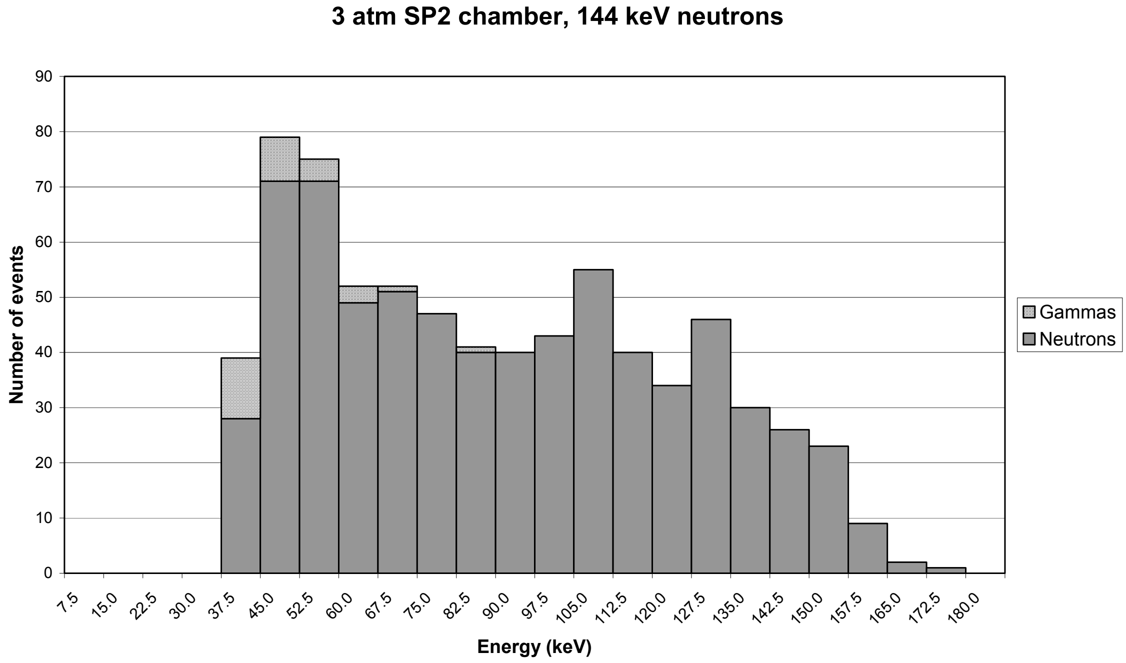

Figure 17. Amplitude distribution, with separated neutron and gamma contributions, for the 3 atmosphere SP2 chamber exposed to 144 keV neutrons.

very low amplitudes and high rise times. They could be due to genuine radiation background in the experimental area, or possibly to non-nuclear causes such as microphony or electrical pickup.

The isolated group of points at 300 – 350 mV in Figure 15 is an artefact due to the clipping of the acquired waveform as it reaches the upper boundary of the oscilloscope's vertical acquisition window. Clearly, measurements made on clipped waveforms will be erroneous, and must be excluded from analysis.

Figure 16 shows the 144 keV neutron data plotted in isolation. A proton recoil edge is evident in the neutron locus, and an energy calibration was derived by assigning an energy of 144 keV to the point halfway down the upper edge of the projected amplitude distribution (about 123 mV).

A neutron / gamma discrimination boundary was set up, as before, using a single sloping line and a threshold at approximately 33 keV (shown in Figure 16). The Figure also shows (dotted line) the approximate position of the threshold that would have to be set for old-style amplitude-based discrimination; the new threshold is lower by about 10 - 15 keV.

The projected amplitude distribution, separated into neutron and gamma contributions, is shown in Figure 17. The approximate resolution, based on the 87.5% - 12.5% interval, is 22%; the fit-based figure of Birch *et al.*, derived from measurements with conventional spectroscopy electronics, is 9% for this counter at 150 keV.

Figure 18 shows the data generated by the test pulser, under the same conditions as Figure 14 but with the 3 atmosphere chamber connected. The amplitude spread is similar to that of Figure 14, and is again comparable to the resolution of the proton recoil edge if the pulser spread is assumed to scale with amplitude.

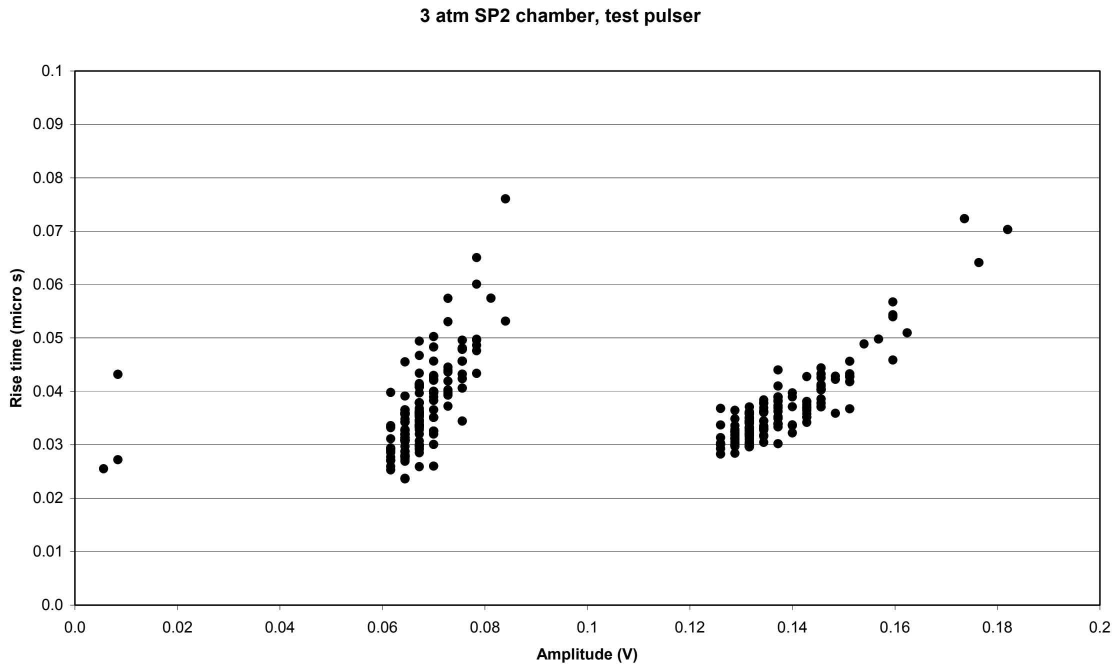

Figure 18. Test pulses measured with 3 atmosphere chamber connected. Again, the rise time was set to 20 ns, and the two amplitudes differ by a factor of two.

3.2.5 Results with 1-atmosphere chamber

The 1-atmosphere chamber from the same set of chambers(6) was mounted at 247.6 cm from the LiF target, at an angle of 50° to the proton beam, and exposed to ^{7}Li(p, n) neutrons as before. The 0°-degree neutron energy was 144 keV, and so the energy of the neutrons striking the chamber was 71 keV (as calculated using the program DROSG-2000(17)).

It was difficult to acquire data successfully with this chamber, as the signals were small, and the oscilloscope frequently triggered on interference or microphony. Figure 19 shows the data that were acquired. A discrimination boundary was set up as before, and a proton recoil distribution derived by projecting the neutron locus on to the amplitude axis. An energy calibration was then determined by assigning an energy of 71 keV to the estimated position of the recoil edge.

The energy of the discrimination threshold, as deduced from the energy calibration, was 21 keV, which is even lower than the 33 keV used with the 3 atmosphere chamber.

The amplitude distribution, with separated neutron and gamma contributions, is shown in Figure 20. The poor statistics mean that the recoil edge is not very well defined, so the estimated resolution (based on the 87.5% - 12.5% interval) of 27% must be regarded with some caution. The resolution measured by Birch et al. for this chamber, with conventional spectroscopy electronics and derived via a fitting technique, is 9% at 72 keV.

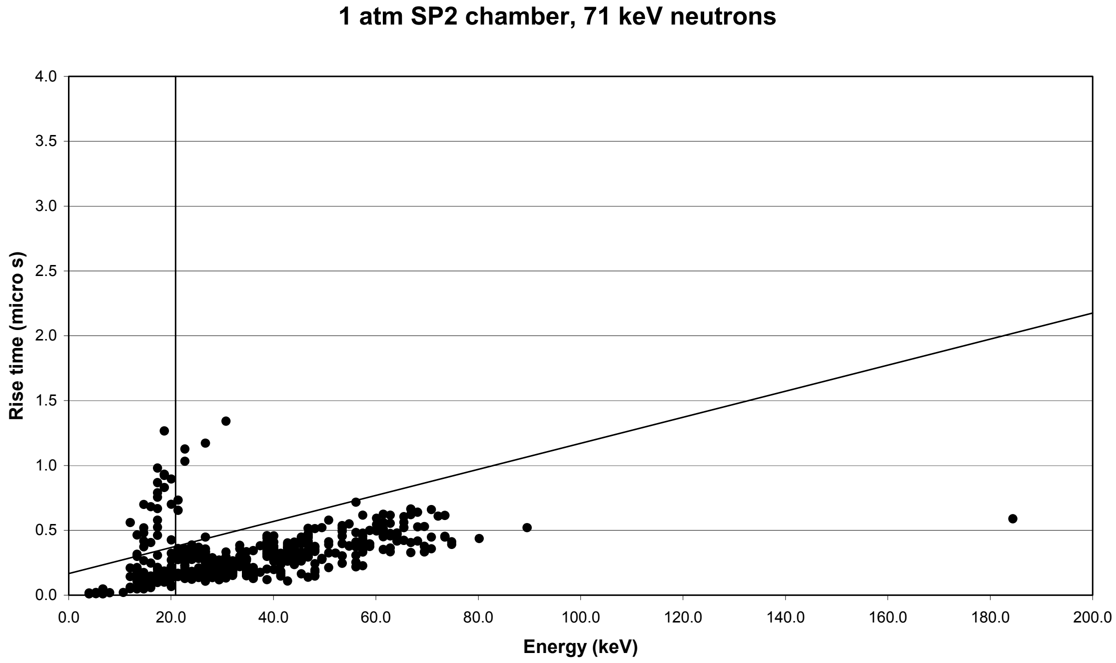

Figure 19. Data for 1-atmosphere chamber exposed to 71 keV neutrons. The solid lines show the discrimination boundary and threshold.

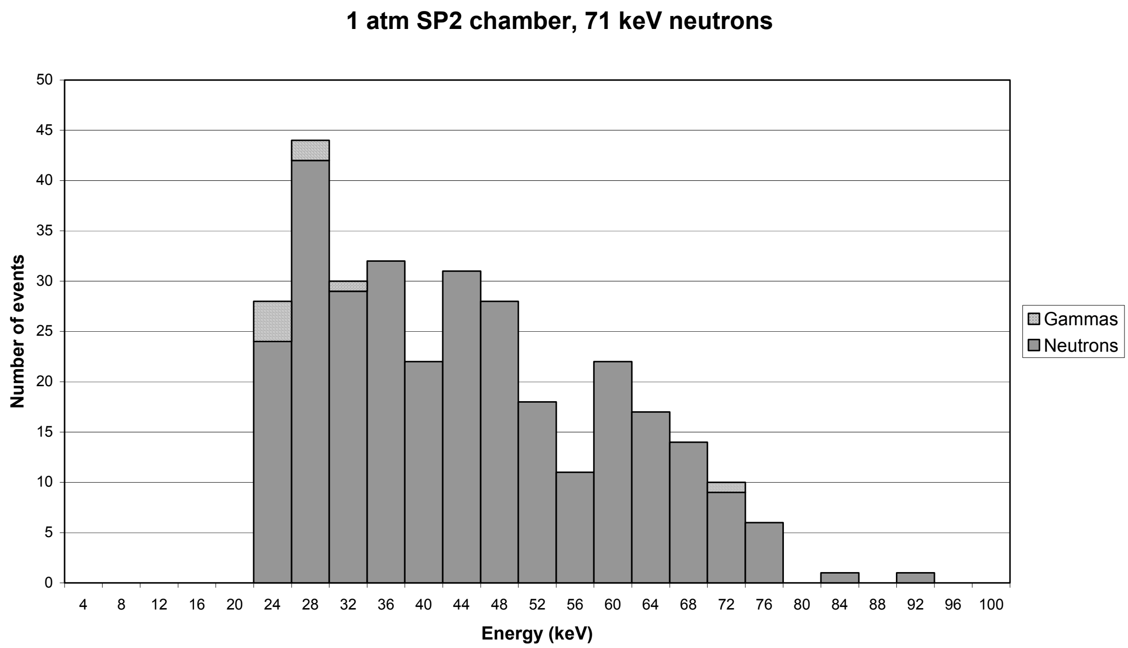

Figure 20. Amplitude distribution, with separated neutron and gamma contributions, for 1-atmosphere chamber exposed to 71 keV neutrons.

3.2.6 Measurements with 3-atmosphere chamber and the NPL Realistic Field

The 3-atmosphere chamber from the set described by Birch *et al.*[(6)] was set up at 454 cm from the D_2O sphere of the NPL Realistic Field facility[(18, 19)], at an angle of 124° to the proton beam. The resulting distribution is shown in Figure 21.

The measured distribution is complex and has some striking features, including a peak at an amplitude of approximately 660 mV, and a curved feature just below 1000 mV. A gamma ray locus is also visible at low amplitudes.

To help in the interpretation of this distribution, data were taken with the Realistic Field facility turned off, and using just the chamber's internal ^{239}Pu alpha calibration source. These are shown in Figure 22, and prove that the parts of the distribution in Figure 21 above about 700 mV are due to the calibration source. (The similarity to Figure 7, showing the pulses from the internal alpha source of the 9-atmosphere NPL chamber, is clear.)

The details of the distribution of alpha points above 1000 mV must be treated with some caution, as the AN302/NL fast amplifier is not linear above this voltage.

The peak at 660 mV must be due to the thermal component of the Realistic Field reacting with the trace of ^{3}He in the chamber, and indeed the energy calibration derived in earlier measurements (when 144 keV was found to correspond to roughly 123 mV) puts the peak at 773 keV, which is a good match to the 764 keV expected for the ^{3}He peak. It is interesting that the peak is not isolated on the low energy side, but instead sits at the high energy end of a large fan-shaped region of points. The reduced-energy points are presumably due to the ion track being cut short by the chamber wall, and for each reduced track length the range of possible orientations gives a range of rise times up to the maximum.

The amplitude spread of the ^{3}He peak, estimated from Figure 21, is roughly 10%. The resolution measured for this peak by Birch *et al.*[(6)], with conventional electronics, was 5.6%.

There is no evidence in Figure 21 of a proton recoil distribution from fast neutrons, and this remained the case even when the chamber was moved from 454 cm to 94 cm from the D_2O sphere. Evidently the high thermal cross section of ^{3}He is allowing the thermal component of the Realistic Field to dominate the fast component.

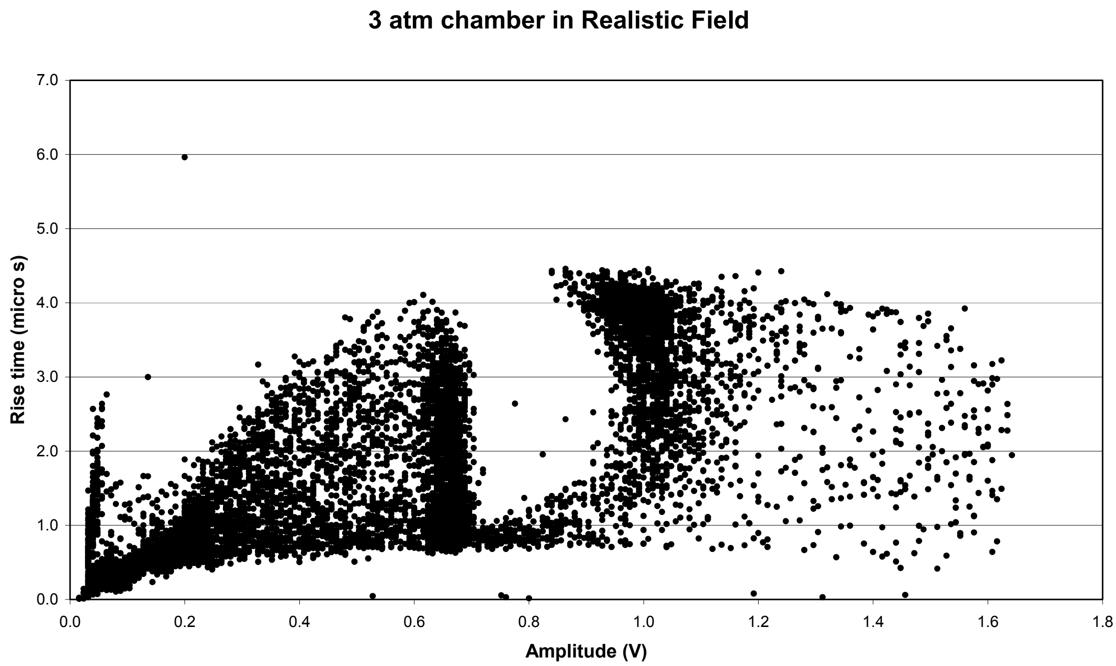

Figure 21. Data measured with 3-atmosphere chamber in NPL Realistic Field

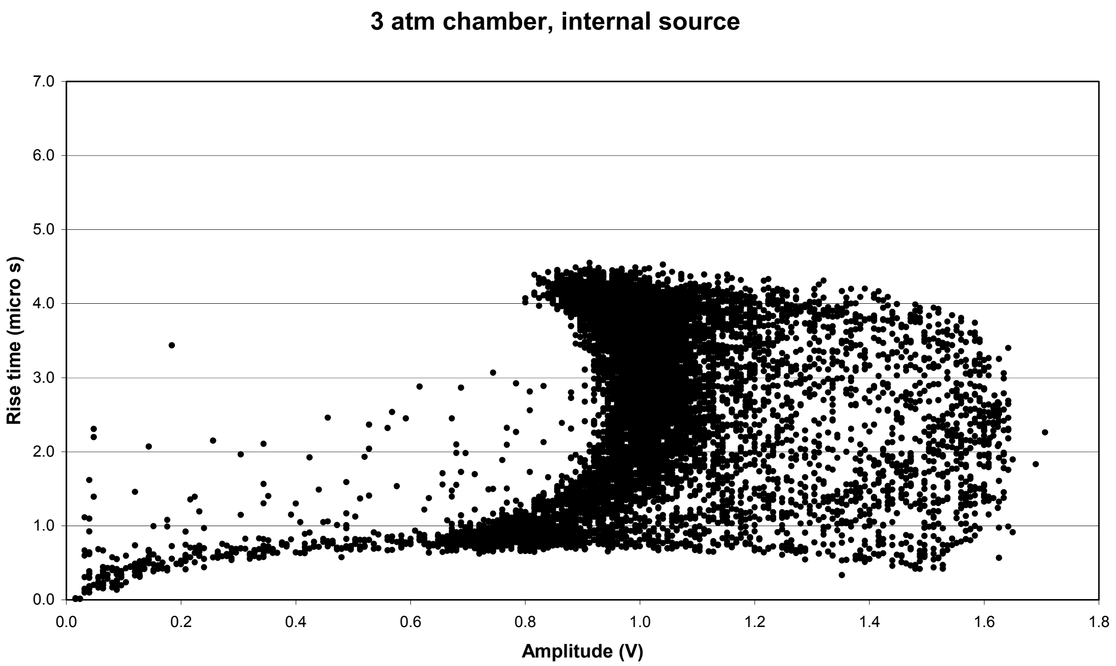

Figure 22. Data from the internal ^{239}Pu calibration source of the 3-atmosphere chamber.

4 Conclusions and Recommendations

The rise times of pulses from SP2 chambers have been measured by digital techniques, and successfully used to discriminate between neutron and gamma events. This discrimination has been extended downward in energy to below 50 keV, where conventional amplitude-based discrimination becomes unreliable. The use of digital techniques allowed the electronics to be very simple, and also provided direct measurements of the pulse rise time. Using a digital oscilloscope with built-in waveform measurement features allowed data to be taken and processed without a great deal of programming effort.

It is clear from the likes of Figure 8 and Figure 21 that there is a great deal of information in the rise time of the pulses. This information is lost when the pulses are processed by traditional pulse height analysis.

In conventional analogue electronics, the modules are carefully designed to reject signals that are outside the expected frequency band. The simple electronic arrangement used in the present work lacked this ability, and made it hard to measure the small signals from the lower pressure chambers in the presence of microphony and electrical interference. Careful choice of the oscilloscope trigger mode was necessary to prevent the acquired data being dominated by unwanted signals.

Furthermore, the measurement algorithms were not optimised for the present application, and may not have carried out the determination of rise time and amplitude in the best way for the particular pulse shapes produced by SP2 chambers, or coped well with unusual events such as pulse pile-up. (As an example of an unusual pulse shape, Figure 23 shows a pulse in which the rate of rise appears to change part way up.) These difficulties may explain why the amplitude resolution of the system was poor, being over twice as broad as that achieved by conventional electronics.

The digital technique shows great promise and merits further development. The chief problems appear to be those of poor amplitude resolution and unwanted signals. To address these, the following steps are recommended:

- Investigate the cause of the poor amplitude resolution. Look at the range of pulse shapes produced by SP2 chambers, and evaluate how well the built-in measurement algorithms cope with these shapes. Also check the response of the system to pulses of known and reproducible shape from a pulse generator.
- Using the results of this investigation, develop measurement algorithms for this application specifically. Include the detection and handling of pulse pile-up if possible. Significant programming effort will be necessary, but it does appear that general-purpose algorithms are not completely satisfactory.
- Move to a hardware platform comprising a plug-in digitiser card in a portable PC, to maximise the portability and adaptability of the system, and free the oscilloscope for other uses.
- Investigate the feasibility of analysing the pulses as they are acquired, so that huge quantities of data are not accumulated. Such rapid processing may require specialised hardware.
- Add hardware filtering (e.g. a high pass R-C filter) in front of the digitiser, so that some unwanted signals are never even digitised.

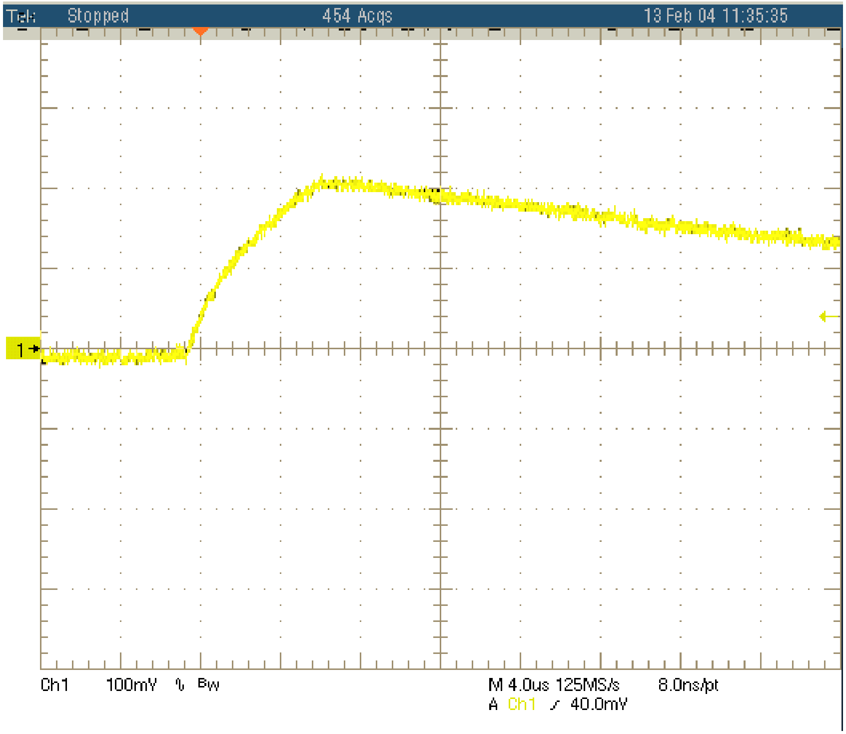

Figure 23. An example of an unusual pulse with two rise times.

If the outstanding problems can be solved, the digital technique holds out the prospect of proportional counter spectrometry, including neutron / gamma discrimination, useable in the field with little more electronics than a portable PC and an HV supply.

5 Acknowledgements

The author is grateful to Graeme Taylor and Neil Roberts for their generous help with setting up the measurements; to David Thomas, Graeme Taylor and Neil Roberts for commenting most helpfully on the manuscript; and to Nigel Watkins for the loan of the DCC system and his expert guidance on using it.

6 References

1. Tagziria, H. and Hansen, W. Neutron spectrometry in mixed fields: proportional counter spectrometers. *Rad. Prot. Dosimetry*, 2003, **107**, 73 – 93.

2. West, D. Energy Measurements with Proportional Counters, *Progress in Nuclear Physics*, edited by O R Frisch, London, Pergamon Press, 1953, 18 – 62.

3. Benjamin, P.W., Kemshall, C.D. and Redfearn, J. The use of a gas-filled spherical proportional counter for neutron spectrum measurements in a zero energy fast reactor. AWRE Report NR 2/64. 1964.

4. Benjamin, P.W., Kemshall, C.D. and Redfearn, J. A high resolution spherical proportional counter. *Nucl. Instrum. Methods*, 1968, **59**, 77 – 85.

5. Tagziria, H. and Thomas, D.J. A high resolution neutron spectrometry system for the 50 to 1500 keV energy region. *NPL Report CIRM 21*, November 1998.

6. Birch, R., Peaple, L.H.J. and Delafield, H.J. Measurement of Neutron Spectra with Hydrogen Proportional Counters, Part 1, Spectrometry System and Calibration. UKAEA Harwell Report AERE-R 11397. October 1984.

7. Berger, M.J., Coursey, J.S., and Zucker, M.A. ESTAR, PSTAR, and ASTAR: Computer Programs for Calculating Stopping-Power and Range Tables for Electrons, Protons, and Helium Ions (version 1.2.2). Available online at: http://physics.nist.gov/Star (National Institute of Standards and Technology, Gaithersburg, MD., 2000.)

8. Verbinski, V.V. and Giovannini, R. Proportional counter characteristics, and applications to reactor neutron spectrometry. *Nucl. Instrum. Methods*, 1974, **114**, 205 – 231.

9. Bennett, E.F. Fast Neutron Spectroscopy by Proton-Recoil Proportional Counting. *Nucl. Sci. Eng.*, 1967, **27**, 16 – 27.

10. Obu, M., Ichimori, T. and Shirakata, K. Gamma-ray discrimination in a proton-recoil spectrometer for a fast reactor spectrum measurement. *Nucl. Instrum. Methods*, 1970, **89**, 131 – 139.

11. Knauf, K. and Wittstock, W. Neutron Spectrometry with Proton Recoil Proportional Counters at the Research and Measurement Reactor Braunschweig – Status of the Technique. Bericht FMRB-114. July 1987.

12. Marsh, J.W., Thomas, D.J. and Burke, M. High resolution measurements of neutron energy spectra from Am-Be and Am-B neutron sources. *Nucl. Instrum. Methods in Phys. Res. A*, 1995, **366**, 340 – 348.

13. Weise, K., Weyrauch, M. and Knauf, K. Neutron response of a spherical proton recoil counter. *Nucl. Instrum. Methods in Phys. Res. A*, 1991, **309**, 287 – 293.

14. Keightley, J.D. and Watt, G.C. Digital Coincidence Counting (DCC) and its use in the corrections for out-of-channel gamma events in 4π β coincidence counting. *Appl. Radiat. Isot.*, 2002, **56** (1 – 2), 205 – 210.

15. Ryves, T.B. and Paul, E.B. The construction and calibration of a standard thermal neutron flux facility at the National Physical Laboratory. *J. Nucl. Energ.*, 1968, **22** (12), 759 – 775.

16. Kolkowski, P. and Thomas, D.J. Measurement of the fast neutron component in the beam of the NPL Thermal Neutron Column using a Bonner sphere spectrometer. *NPL Report CIRM 28*, May 1999.

17. Drosg, M. DROSG-2000: Neutron source reactions, version 2.2, January 2003. Institute for Experimental Physics, University of Vienna, Austria. Online reference: www-nds.iaea.or.at/drosg2000

18. Thomas, D.J., Horwood, N. and Taylor, G.C. Neutron dosemeter responses in workplace fields and the implications of using realistic neutron calibration fields. *NPL Report CIRM 27*, March 1999.

19. Taylor, G.C., Thomas, D.J. and Bennett, A. A Realistic Field facility to simulate reactor spectra. *Rad. Prot. Dosimetry*, 2004, **110**, 111 – 115.